True intrinsic mechanical behaviour of semi-crystalline and amorphous polymers: Influences of volume deformation and cavities shape

Marc Ponçot, F. Addiego, Abdesselam Dahoun

True intrinsic mechanical behaviour of semi-crystalline and amorphous polymers: influences of volume deformation and cavities shape.

M. Ponçot[1,*], F. Addiego[2], A. Dahoun[1].

[1] *Science and Engineering of Materials and Metallurgy Department, Jean Lamour Institute, UMR 7198 CNRS-Nancy Université / Ecole des Mines de Nancy, Parc de Saurupt, CS 14234, 54042 Nancy cedex, France*

[2] *Advanced Materials and Structures Department, Public Research Centre Henri Tudor, 66 rue du Luxembourg, BP 144, L-4002 Esch-sur-Alzette, Luxembourg*

** Author to whom correspondence should be addressed*

Abstract: A model enabling the determination of the intrinsic mechanical constitutive equations of uniaxially stretched polymers is presented. This model takes into account the cavitation-induced volume strain which can occur during the deformation of such materials. In particular, the true intrinsic axial stress and strain depends on the overall volume strain and a form factor depicting the evolution of the voids shape. Based on our model, the true intrinsic behaviour of high-density polyethylene (HDPE), polypropylene / ethylene-propylene rubber (PP/EPR), and polyethylene terephtalate (PET) was assessed in tension. Compared to the overall true behaviour, the intrinsic true behaviour of the materials did not exhibit anomalies at large strain levels with changing experimental parameters (strain rate and temperature), and can be accurately predicted by means of phenomenological constitutive equations as the one proposed by G'sell and Jonas (1979).

Key words: amorphous polymer, semi-crystalline polymer, toughened blend, uniaxial tension test, volume damage, cavities shape, corrective form factor, intrinsic true mechanical behaviour.

1. Introduction:

Thermoplastic polymers are currently representing a great issue for various actors of the industry to manufacture irregular shaped pieces requiring advanced mechanical properties. This is particularly the case for the automotive industry where the demand in thermoplastics increases due to their high toughness, coupled with their low density that enables to address environmental specifications (Ponçot, 2009). Depending on its formulation (homo-polymer, copolymer, branching, use of reinforcing agents…) and on its microstructure (amorphous, semi-crystalline...), a given thermoplastic can exhibit a wide range of end-use mechanical properties. Accordingly, it is of high interest to identify, analyse, and predict with precision the thermo-mechanical behaviour of thermoplastics.

The deformation mechanisms of polymers depend on their initial microstructures which are mainly induced by the formulation and the conformation processes. As a result, mechanical behaviour presents significant differences if the polymer matrix is amorphous (Boyce and Arruda, 1990; Bartczak *et al.*, 1996; Steenbrink *et al.*, 1997; Vigny *et al.*, 1999; Ponçot *et al.*, 2011), semi-crystalline (G'sell *et al,*. 1997; Amornsakchai *et al.*, 2000; G'sell *et al.*, 2002; Addiego *et al.*, 2006; Séguela, 2007; Galeski and Rozanski, 2010; Ponçot *et al.*, 2009) or filled with rubber particles (Bucknall *et al.*, 1972; Pukansky *et al.*, 1994; Plummer *et al.*, 1996; van der Wal and Gaymans, 1999; Nitta *et al.*, 2008; Mae *et al.*, 2008; Ponçot,

2009). Chain orientation, shear banding, and damage are the main involved deformation micromechanisms whatever the initial microstructure of the considered material. The prevalence of one mechanism regarding the others induces such kind of mechanical properties differences.

Although the micromechanisms of deformation of polymers are currently well described as a function of the microstructure, a quantitative inelastic modelling is still lacking. Such predictive model would facilitate the understanding of the relationship between macroscopic behaviour and micromechanisms of deformation. Over the past three decades, several constitutive models were proposed to assess the elastic-viscoplastic deformation behaviour of solid polymers:

i) Phenomenologically-based models: Due to the difficulty to implement the elementary deformation mechanisms in the constitutive equations, some authors relied on purely phenomenological models (G'sell and Jonas, 1979; G'sell and Dahoun, 1995; Chaboche, 1995; G'sell *et al.*, 1997 and 1999; Khan and Zhang, 2001; Khan *et al.*, 2006; Zaïri *et al.*, 2007; Regrain *et al.*, 2009). These last authors fitted the nonlinear behaviour of semi-crystalline polymers by specific mathematical functions taking into account external factors as strain rate and temperature.
ii) Physically-based models: As an alternative, the physical approach was recently illustrated by Boyce *et al.* (2000) describing the elastic-viscoplastic behaviour of amorphous polyethylene terephthalate above its glass transition and integrating the strain rate dependence. This model was then extended by Azhi *et al.* (2003) and Richeton *et al.* (2007), taking into account the strain-induced crystallization. Other macroscopic inelastic constitutive models for various semi-crystalline polymers were recently proposed by Nikolov *et al.* (2006) and Ayoub *et al.* (2010 and 2011). In their representation, the material was considered as an aggregate of two-phase layered composite inclusions which are randomly oriented. These models simulated the macromolecular chains orientation but did not consider the volume damage.

However, as it has been expressed first by Gurson (1977) then by Tveergaard (1981) and Lemaitre (1996), the determination and the introduction of the volume deformation in the expression of the true stress and strain are essential to provide efficient mechanical constitutive equations. Detrez *et al.* (2011) used a model based on the damage mechanics framework introducing a macroscopic damage variable and not the void volume fraction as indicator of damage. Investigations based on the Gurson-type description of porous materials provided mechanical behaviours caption first limited to spherical voids (Steenbrink *et al.*, 1997; Laiarinandrasana *et al.*, 2009; Zaïri *et al.*, 2005 and 2008). Recently Zaïri *et al.* (2011) developed a model considering the evolution of voids shape. In particular, voids were first supposed spherical at the onset of cavitation, and then with increasing strain level voids evolved into ellipsoids with major axis oriented along tensile direction. The gradual orientation of the macromolecular chains, the voids shape evolution and the overall volume variation were successfully implemented in the mathematical formulation of the constitutive model. Therefore, it is of high importance to accurately describe the anisotropic growth of voids, using physically realistic damage models such as the one proposed by Gologanu *et al.* (1997).

This paper focuses on the achievement of the true intrinsic expressions of stress and strain during the tensile deformation based on the evolution of void fraction and shape developing in the materials. To this end, three thermoplastics presenting different microstructures were studied: amorphous polyethylene terephthalate (PET), semi-crystalline high-density

polyethylene (HDPE) and isotactic polypropylene filled with ethylene-propylene rubber particles (PP/EPR). Void fraction (or volume damage) was calculated *in situ* during the stretching procedure, while the voids shape evolution was determined from *post mortem* microscopic observations. The influence of strain rate and temperature on the intrinsic true mechanical behaviour of these three polymers was also investigated. The intrinsic behaviour of the materials was compared to that obtained by simulation using the phenomenologically-based model introduced by G'sell and Jonas (1979). A comparison between the equivalent true intrinsic mechanical behaviours deduced from different deformation paths using the Von Mises plastic criterion was proposed.

2. Experimental section:

2.1. Materials

Polyethylene terephtalate

As amorphous thermoplastics, we selected a grade of polyethylene terephtalate (PET) that was supplied by Eastman (Voridian PET 9921). Its average molecular weight is $\overline{M}_w$ = 51 000 g.mol^{-1}, while its polydispersity is 2 (Ponçot *et al.*, 2011). It was processed by extrusion into 5 mm-thick plates. Differential scanning calorimetry results, at a standard heating rate of 10 °C.min^{-1}, show a glass transition temperature of about 75 °C, a melting temperature of 240 °C and a cold crystallization temperature of 155 °C. The initial amount of crystallinity of PET is equal to 0 since the enthalpies of cold crystallization and fusion compensate one each other. Wide-angle X-ray scattering (WAXS) analysis confirms that these PET plates have an amorphous microstructure and an isotropic distribution of the chains whatever the spatial direction.

High density polyethylene

As semi-crystalline thermoplastic polymer, a grade of high-density polyethylene (HDPE) manufactured by DuPont Canada (ref. Sclair 2907) was chosen. Its number and weight average macromolecular weights, determined by previous authors (e.g. Amornsakchai *et al.*, 2000) are equal to $\overline{M}_n$ = 16,800 g.mol^{-1} and $\overline{M}_w$ = 93,600 g.mol^{-1}. Solid cylinders, 110 mm in diameter, were extruded by the Plastifab Company (Montréal, Canada). In this process, the material is slowly cooled in air after getting out of the die in order to minimize internal stresses and favour homogeneous microstructure. 7 mm-thick plates are cut out of the core region of the cylinders along planes parallel to the extrusion axis. Differential scanning calorimetry results, at the standard heating rate of 10 °C.min^{-1}, show a glass transition temperature close to - 120 °C, a melting temperature of 135 °C. The weight index of crystallinity is found to be equal to 78 wt. % (hydrostatic weighting and differential scanning calorimetry) or 76 vol. %. The crystalline morphology is characterized by spherulites of about 50 µm in diameter composed with regularly twisted lamellae. The long period of the semi-crystalline stacks, as determined by small-angle X-ray scattering, is equal to 27.3 nm that gives, in conjunction with the crystallinity ratio, an average lamella thickness of 20.7 nm. The high crystallinity and coarse microstructure of this HDPE, already investigated by previous authors (Wunderlich, 1973; Addiego, 2006), are due to its very low content in catalytic residues and the absence of nucleating agents.

Polypropylene / ethylene-propylene rubber

As engineering thermoplastic, we selected a polypropylene / ethylene-propylene rubber (PP/EPR) that was supplied by Total Petrochemicals (ref. PPC 3650). The samples were processed by injection moulding into 4 mm-thick plates. The amount of EPR mixed with the PP matrix is 17 wt. %. The final blend presents the following average molecular weights: $\overline{M}_n$ = 69,000 g.mol^{-1} and $\overline{M}_w$ = 599,000 g.mol^{-1} (Ponçot, 2009). Differential scanning calorimetry analysis, at standard heating rate of 10 °C.min^{-1}, reveals two melting peaks. The first one at 115 °C corresponds to the melting of polyethylene crystals. The second one at 167 °C is attributed to the fusion of PP crystals of the α-crystalline phase. The polyethylene lamellae are identified and localized inside the EPR nodules. It means that these particles have a core-shell shape. This characteristic has been previously demonstrated by scanning and transmission electron microscopy (Ponçot, 2009). The glass transition temperature of the PP matrix is close to 10 °C. The elastomeric phase shows a glass transition at - 40 °C. Typical

diameter of these nodules is about 10 µm. Furthermore, additional analyses by wide-angle X-ray scattering inform that the average crystallinity index of PP matrix is 45 vol. %. The long period of the semi-crystalline PP stacks, as determined by small-angle X-ray scattering (SAXS), is equal to 19.1 nm that gives, in conjunction with the volume index of crystallinity, an average lamella thickness of 8.6 nm.

2.2. Measurements

Mechanical testing

The video-controlled mechanical testing method used in this paper, VidéoTraction™, gives access to the true mechanical behaviour of polymers for different deformation paths from video measurements performed locally in the middle of the sample. As a result, the development of necking is taken into account in the measured mechanical behaviour. To ensure the localization of the plastic deformation (necking) at the centre of the sample, a slight geometrical defect is machined out in the middle of the gauge length of the dumbbell-shaped specimen (reduction of 6 % of the specimen width). This specific analysed region is called Representative Volume Element (RVE). The axial true strain in the RVE, ε_{33}, is obtained by a polynomial interpolation of partial strains measured from the displacement of axial markers using Lagrange Transform and following Hencky's definition. For uniaxial tensile testing, the transverse strains in the RVE, ε_{11} and ε_{22}, are equal if the strain field is transversally isotropic in the centre of the neck (Bucknall *et al.*, 1972; Naqui and Robinson, 1993; Pukansky *et al.*, 1994; G'sell *et al.*, 2002; Addiego *et al.*, 2006; Ponçot, 2009). Lastly, the volume strain in the RVE, ε_v, is simply computed from the trace of the true strain tensor:

$$\varepsilon_v = \varepsilon_{11} + \varepsilon_{22} + \varepsilon_{33} \qquad (1)$$

The volume strain can be positive, null or negative. In particular, when it is superior to zero we call it volume damage (since the "reversible" elastic part keeps weak and can be neglected), and in the opposite case (when it is negative) we consider that a compaction mechanism is active.

The axial true stress (Cauchy stress) is determined in the same RVE as the load per unit actual cross-section:

$$\sigma_{33} = \frac{F}{S_0}\exp(-2\varepsilon_{11}), \qquad (2)$$

where S_0 is the initial cross-section of the tensile specimen.

More details about the used methodology can be found in previous papers (G'sell *et al.*, 1992; G'sell *et al.*, 2002; Addiego *et al.*, 2006; Ponçot, 2009, Ponçot *et al.*, 2011). Note that VidéoTraction methodology enables to perform tensile testing at constant axial strain rate.

All the mechanical tests are performed at 30 °C in case of PP/EPR in order to study the influence of the true strain rate (10^{-2} s^{-1}, 5.10^{-3} s^{-1} and 5.10^{-4} s^{-1}). For HDPE, tests are done at three different temperatures (25 °C, 40 °C and 45 °C) at a constant strain rate (10^{-3} s^{-1}). For PET, the selected temperature is 50 °C to stretch samples in the glassy state at three different strain rates (5.10^{-3} s^{-1}, 5.10^{-4} s^{-1} and 5.10^{-5} s^{-1}). The deformation rates were chosen in such a way to ensure a good regulation of the testing machine actuator and to avoid any self-heating of the material during the mechanical testing.

Scanning electron microscopy

Scanning electron microscopy (SEM) is used to observe the microstructure of the materials, and hence, to identify the strain-induced deformation micro-mechanisms. To this end, *Post Mortem* micrographies are recorded using an environmental Quanta FEG 600 electron microscope from FEI Company. The advantage of this equipment is its ability to work under a wide range of saturated vapour pressures. Accordingly, no more sample metallization is necessary to avoid charging effect at the surface of insulating material. The selected microscope parameters are: water vapour pressure of 100 Pa and acceleration voltage of 5 kV. Most of the images were recorded with the secondary electrons detection mode (large field detector). Prior observations, all the samples were submitted at their core to a chemical etching in order to reveal their microstructure. This treatment consists in eliminating heterogeneous layer induced by the cutting procedure and all other artefacts (Olley *et al.*, 1982). The chosen solution is a mixture of sulphuric acid, orthophosphoric acid and potassium permanganate powder. Polymer samples were soaked during 5 hours using a magnetic stirrer. Then, they were rinsed successively in hydrogen peroxide, distilled water and pure ethanol.

Optical microscopy

In transmission mode, this technique is used to observe the volume damage in case of a translucent material such as amorphous PET. *Post mortem* observations are conducted after recovery of the stretched sample and are performed on 20 µm-thick slices cut using a microtome. These samples are taken of the center of the neck where the RVE is localized.

3. Experimental results:

3.1. *True mechanical behaviours of PP/EPR and PET as a function of true strain rates*

This study is conducted on the two polymers PP/EPR and PET. Figure 1 shows the true mechanical curves of these two materials obtained by the VideoTraction™ system in tension for three different true strain rates. For both materials, an increase of stress is observed up to moderate strain levels with increasing the stretching rate. The yield point is higher in the case of PET than in the case of PP/EPR whatever the studied strain rate. After the yield point, different amplitudes of softening appear between these two polymers, since PP/EPR is semi-crystalline and stretched at a temperature higher than its glass temperatures ($T_{g\ PP}$ = 10 °C and $T_{g\ EPR}$ = - 45 °C) and PET is amorphous and stretched in its glassy state (T_g = 75 °C). Then, plasticity stage is characterized by a quite large plateau. Finally, strain-hardening takes place up to large strain level. However, during the strain-hardening stage, the stress-strain curves are not parallel anymore for the two materials, as indicated in figure 1. This phenomenon does not enable to predict the tensile behaviour at large strain level using phenomenological constitutive equations as the one proposed by G'sell and Jonas (1979).

3.2. *True mechanical behaviours of HDPE as a function of temperature*

HDPE specimens are uniaxially stretched at three different temperatures (25°C, 40°C and 45°C) in the rubber state since its glass temperature is of about -120°C. Results are presented in figure 2. It is to be noted that the tensile curves of HDPE are similar to that of PP/EPR and includes a weak softening stage. As expected, stress increases with decreasing temperature up to moderate strain level. However, as noted for PET and PP/EPR, for high strain level, true stress-strain curves obtained for the different temperatures cross each other, which does not permit their simulation.

3.3. Damage mechanisms: volume strain and voids shape

By means of a 2D video extensometer, the volume strain is evaluated *in situ* at the macroscopic scale using equation 1. Figures 3 and 4 present the curves collected for PP/EPR, PET and HDPE. The influence of strain rate and temperature is quite similar on the development of volume damage for the three different materials (figures 3 and 4). In particular, the volume deformation increases with strain rate and decreases with temperature. In figure 3, for PP/EPR and PET, curves present the same evolution with the axial true strain whatever the strain rate. This means that similar voids in terms of shape develop inside each material. Polymers stretched in the glassy state, such as the amorphous PET, show the highest amount of voids. At very large strain values, we can note differences between the volume strain behaviours of PP/EPR and PET. In the first case (figure 3 a)), we observe a plateau followed by a slight decrease. For PET (figure 3 b)), linearity keeps constant until failure of the tensile specimen.

In the case of HDPE (figure 4), the volume strain is lower than that of the two previous materials whatever the strain level. This is due to the fact that HDPE is stretched in a highly viscoelastic state (T_{gHDPE} = - 120 °C). As previously exposed by Addiego *et al.* (2006), a slight compaction is observed during the first step of plasticity at the highest temperature (45 °C). This unusual phenomenon of compaction is mainly caused by the strain-induced chain orientation of amorphous phase that is facilitated with increasing temperature, while cavitation mechanisms are hindered (Addiego *et al.*, 2006).

To identify the morphology of the cavities developing within the materials during the plastic deformation by stretching, *post mortem* microscopic observations were made after the viscoelastic recovery. Figure 5 shows the RVE microstructure of PP/EPR after stretching procedure at 30 °C and 5.10^{-3} s^{-1} up to the axial true strains of 0.3, 0.5 and 1.4.

These SEM micrographies exhibit quite large cavities induced by the tensile test. It appears that volume damage mostly takes place inside the EPR nodules due to their core-shell microstructure (Mae *et al.*, 2008; Ponçot, 2009). Indeed, stresses concentration localized around the particles are transferred to the extremities of their internal rigid part made of independent PE crystalline lamellae. Voids show an evolution of their shape from a spherical state (micrographies a) and b) of figure 5) to an ellipsoidal state similar to cigars (micrography c) of the figure 5) because it was previously shown that the EPR nodules align along the stretching direction (van der Wal and Gaymans, 1999). Close to the sample breaking, the PP/EPR microstructure is highly fibrillar.

In the case of glassy PET, an important dilatation is recorded (Figure 3 b)) and is correlated with the development of crazes as shown in figure 6 and previously enlightened by the past (Vigny *et al.*, 1999; G'sell *et al.*, 2002). The nucleation of this kind of damage begins once the yield stress is reached. Figure 6 presents two optical micrographies of the RVE of PET specimens stretched at 50 °C and 5.10^{-5} s^{-1} up to the axial true strain values of 0.45 and 1.2. Crazes oriented perpendicular to the stretching direction are observed. At 45 degrees of the mechanical solicitation direction, we can notice the presence of shear bands which link the extremities of crazes. Note that crazes formed during the test do not show a significant opening until the rupture of the sample. A gradual multiplication and coalescence of the crazes occur until the sample breaking (Ponçot *et al.*, 2011). For this material, we consider that voids have a constant shape whatever the strain level. Voids can be modeled by discs (penny-shaped voids).

Figure 7 is a set of SEM micrographies of HDPE specimens stretched at 25 °C and 10^{-3} s^{-1} up to true strain values of 0.29, 0.48 and 1.3. Due to the specific morphology of spherulites encountered in HDPE (twisted lamellae), the process of cavitation is quickly characterized by a very important amount of spherical voids which finally do not much elongate themselves until the rupture of the sample. So, figure 7 reveals mainly bubble-shaped voids (Addiego, 2006; Addiego *et al.*, 2006 and 2011).

From these numerous micrographies reported in the figures 5, 6 and 7, it is possible to express additional comments on the evolution of the slope of the curves $\varepsilon_v = f(\varepsilon_{33})$ of figures 3 and 4. In the case of HDPE (once the compaction phenomenon is over) and PET, the quasi constant and positive slope value means that cavities shape does not significantly evolve during the deformation. Voids keep a spherical shape in the case of HDPE and a penny shape in case of PET whatever the temperature and the strain rate, respectively. On the contrary, in case of PP/EPR, a decrease of this slope is observed for high strain levels. Elongated cavities continue to grow with the deformation but essentially in one direction: the stretching direction. As a consequence, this phenomenon induces a slight closure of the width of the cigars. It is attributed to a highly fibrillar microstructure of the stretched polymer.

4. Discussion:

Our results show the influence of the true strain rate and temperature on the true mechanical behaviour and volume strain of PP/EPR, PET and HDPE. Many authors reported the strong competition between two main micro-mechanisms of plastic deformation which are the orientation of the macromolecular chains and the volume damage in the case of amorphous and semi-crystalline polymers stretched in tension (Ward, 1971; Samuels, 1971 and 1974; Plummer *et al.*, 1996; Dahoun, 2004; Ponçot, 2009, Ponçot *et al.*, 2011; Martin *et al.*, 2011). For the three studied materials of this paper, true mechanical behaviours curves are well stackable (using a constant shift factor to the stress values) until the plastic plateau. Then, crosses between curves appear which means that one micro-mechanism of plastic deformation prevails over the other one depending on the mechanical test parameters (strain rate and/or temperature). Raw data collected by the VideoTraction™ system (figures 1 and 2) does not take into account the microstructure evolution induced by the mechanical solicitation. But, the simultaneous observation of the true stress – strain curve and volume strain – true strain curves leads to discuss about the influence of the mechanical test parameters on the involved micro-mechanisms of deformation. Intersections between the curves are due to an increase of the true stress values in the case of the lowest true strain rate and highest test temperature (Figures 1 and 2) at the onset of strain-hardening. Regarding figures 3 and 4, this hardening stage is induced by an important orientation of the macromolecular chains along the tension direction when the amount of volume damage is the lowest. Consequently, curves of figures 1 and 2 inform us about the true mechanical behaviour of a new material which can be assimilated to a composite: a polymer matrix "filled" with voids. In order to exclusively characterize the mechanical properties of the polymer matrix alone, it is determinant to take into account the volume deformation in the calculation of the true strain and the true stress variables since specimen section changes during the test. Therefore, the determination of the true intrinsic mechanical behaviours presents a great interest and constitutes the rest of this paper. The influence of the stress triaxiality effect (mechanical concept of necked specimens introduced by Bridgman in 1952 and Beremin in 1980 on metals) is neglected in this work since it is maximal at small strain values close to the yield point and the structural softening of the material, while the volume strain is weak at the same time. A few measurements of this triaxiality phenomenon were obtained on the three studied materials on the basis of the Bridgman hypothesizes. They have shown weak deviations between the true stress and the true effective stress of about 5 %. In this work, we focus our attention on the correction of the curves at large strains once necking is activated and where the volume strain is high. An extension to large strain and damage based model was discussed in a very recent paper of Boisot *et al*, (2011), where comparison of the experimental results with finite element computations was carried out. It was shown that the triaxiality ratio gradually decreases from the yield point (onset of necking) to strain-hardening stage (end of necking).

4.1. Equations of the true intrinsic stress and strain

As the damage always occurs simultaneously with elastic and plastic strains, their classical variables must be taken into consideration. The strain tensor can be defined as follows:

$$[\varepsilon] = [\varepsilon_{el}] + [\varepsilon_{pl}] \quad (3)$$

where $[\varepsilon_{el}]$ and $[\varepsilon_{pl}]$ denote the elastic and the plastic strain tensors, respectively.

Each part of this relationship shows a contribution of the volume variation which is important to quantify (Lemaître, 1996):

$$[\varepsilon] = [\varepsilon^{i}_{el}] + [\varepsilon^{v}_{el}] + [\varepsilon^{i}_{pl}] + [\varepsilon^{v}_{pl}] \quad (4)$$

where $[\varepsilon^{v}_{el}]$ and $[\varepsilon^{v}_{pl}]$ denote the elastic and the plastic volume strain tensors, respectively.

Depending on the situation, a constant volume deformation is called “isochoric deformation”, “conservative deformation”, “deviatoric deformation” or “intrinsic deformation”. The remainder is named “volume deformation” and it can be either isotropic or anisotropic. It is useful to write:

$$Tr\left([\varepsilon^{i}_{el}]\right) = \varepsilon^{d}_{11\ el} + \varepsilon^{d}_{22\ el} + \varepsilon^{d}_{33\ el} = 0 \quad (5)$$

$$Tr\left([\varepsilon^{v}_{el}]\right) = \varepsilon^{v}_{11\ el} + \varepsilon^{v}_{22\ el} + \varepsilon^{v}_{33\ el} = \varepsilon^{v}_{el} \neq 0 \quad (6)$$

and

$$Tr\left([\varepsilon^{i}_{pl}]\right) = \varepsilon^{d}_{11\ pl} + \varepsilon^{d}_{22\ pl} + \varepsilon^{d}_{33\ pl} = 0 \quad (7)$$

$$Tr\left([\varepsilon^{v}_{pl}]\right) = \varepsilon^{v}_{11\ pl} + \varepsilon^{v}_{22\ pl} + \varepsilon^{v}_{33\ pl} = \varepsilon^{v}_{pl} \neq 0 \quad (8)$$

Elastic volume strain:

Volume deformation in the elastic zone is due to the material compressibility (dilatation and contraction of the macromolecular chain bonds). There is not cavity created during this first stage of deformation. In tension, the elastic volume deformation is expressed by:

$$\varepsilon^{v}_{el} = \frac{\sigma_h}{K} = \frac{\sigma_{33}}{3\,K} \quad (9)$$

where K is the consistency of the material and σ_h the hydrostatic stress.

The initial part of the curve ε_v - ε_{33} is linked to the Poisson’s coefficient, ν, by:

$$\varepsilon^{v}_{el} = (1 - 2\nu)\ \varepsilon_{33\ el} \quad (10)$$

Finally, a spherical tensor is obtained since the hydrostatic stress is isotropic and our polymer materials all present a Poisson ratio close to 0.35:

$$[\varepsilon^{v}_{el}] = \begin{bmatrix} (1-2\nu)\sigma_{33}/3E & 0 & 0 \\ 0 & (1-2\nu)\sigma_{33}/3E & 0 \\ 0 & 0 & (1-2\nu)\sigma_{33}/3E \end{bmatrix} \quad (11)$$

where E is the Young’s modulus of the material.

Plastic volume strain:

It is considered that the plastically deformed and damaged material is a composite system characterized by two distinct phases: matrix and cavities (figure 8). Then, true stress and strain can be expressed as follows in the particular case of this composite (Lemaître, 1996):

$$[\sigma] = (1-f^{v}).[\sigma^{i}] + f^{v}.[\sigma^{v}] \quad (12)$$

$$[\varepsilon] = (1-f^{v}).[\varepsilon^{i}] + f^{v}.[\varepsilon^{v}] \quad (13)$$

where f^v is the cavity fraction created inside the material, σ^i and ε^i are the intrinsic true stress and strain (of the polymer matrix without voids), respectively.

The evolution of $\sigma_{33}{}^i$ as a function of $\varepsilon_{33}{}^i$ represents the true intrinsic mechanical behaviour of the solid polymer without cavities. Their expressions, based on the volume deformation and the voids shape, are presented hereafter.

4.2. Introduction of a β-factor taking into account the cavities shape developing during plastic strain.

It is relevant to introduce a shape factor, β, linked to the cavity geometry present inside the polymer matrix based on the relation: $\varepsilon_{33}^i = \varepsilon_{33} - \gamma\varepsilon_v$ where $\gamma = \frac{1}{2\beta+1}$ and $\beta = C_3/C_1$. $C_{i=1,2,3}$ represents the geometrical dimensions of a cavity in the three directions of space taking the axis 3 as the tensile direction. Since during a tension test, the hypothesis of transversal isotropy is always verified, the equality of the parameters C_1 and C_2 characterising the cavities dimensions in the two transversal directions is systematically verified.

Three main cavities morphologies can be considered as illustrated in figure 9:

- Crazes which are developed perpendicularly to the stretching direction ($\beta \to 0$),
- Spherical bubbles ($\beta \to 1$),
- Tubes elongated in the tension test direction ($\beta \to \infty$).

In the case of the formation of crazes, the specimen was only stretched in the tension direction without transversal contraction. The volume deformation tensor presents an only non-null component such as: $\varepsilon_{11}^v = \varepsilon_{22}^v = 0$; $\varepsilon_{33}^v = \varepsilon_v$. The intrinsic true strain is hence equal to: $\varepsilon_{33}^i = \varepsilon_{33} - \varepsilon_v$. The section of the specimen which endures the load remains unchanged and the intrinsic true stress is expressed by: $\sigma_{33}^i = \sigma_{33}$.

In case of spherical cavities, the deformation is isotropic and volume strain tensor is composed with: $\varepsilon_{11}^v = \varepsilon_{22}^v = \varepsilon_{33}^v = \frac{\varepsilon_v}{3}$. The intrinsic true strain is $\varepsilon_{33}^i = \varepsilon_{33} - \frac{\varepsilon_v}{3}$. The axial component of the intrinsic true stress is written: $\sigma_{33}^i = \frac{F}{S^i} = \sigma_{33}\frac{S}{S^i} = \sigma_{33}\exp\left(\frac{2}{3}\varepsilon_v\right)$ where S and S^i are the areas of the unstretched and stretched material section, respectively, and F is the applied load.

The last remarkable shape of cavities is tube-like shape. These elongated voids in the tension direction show a large length C_3 in comparison with their lateral dimensions. It is considered that they do not endure transversal contraction. In this case components of the volume deformation tensor can be written: $\varepsilon_{11}^v = \varepsilon_{22}^v = \frac{\varepsilon_v}{2}$; $\varepsilon_{33}^v = 0$. The intrinsic true strain in the axial direction is: $\varepsilon_{33}^i = \varepsilon_{33}$. The expression of the intrinsic true stress is given by: $\sigma_{33}^i = \frac{F}{S^i} = \sigma_{33}\frac{S}{S^i} = \sigma_{33}\exp(\varepsilon_v)$.

These relations show that depending on the value of the volume damage, the intrinsic behaviour of the material is more or less different from the overall one. In the case of a

positive volume deformation, the polymer has an intrinsic true strain inferior to the global strain and an intrinsic true stress superior to the macroscopic stress.

Figure 10 a) illustrates the influences of the different remarkable values of the β factor on the final intrinsic true mechanical behaviour of the HDPE stretched at three different temperatures. The introduction of the cavities shape in the correction of the true stress and strain should bring a higher accuracy in the assessment of intrinsic behaviour of the material.

It appears that whatever the chosen β factor, cavities shape does not significantly influence the mechanical behaviour until the beginning of the plasticity. It is mainly due to the low values of the volume deformation until this stage (figure 4 a)). So, the first stage of the cavitation process (crazing), when it occurs, can always be neglected. Then, all the curves converge again at the highest true strain values what means that the progressive elongation of the voids in the tensile axis does not affect a lot the final intrinsic mechanical behaviour of HDPE. The most important effect of the cavities shape on the true mechanical behaviour occurs during the plastic plateau and the initiation of the strain-hardening ($0.35 < \varepsilon_{33} < 1.2$).

In the previous work of Addiego (2006) which deals with tension tests of HDPE, a relation of the beta factor as a function of the volume strain was given (figure 10 b)): $\beta = \exp(4\varepsilon_v - 1)$. We notice that the voids shape evolves with stretching as previously discussed since beta value changes from 0.4 to 1.4. This result indicates a weak elongation of the voids along tensile direction during the plastic deformation and confirms the fact that taking a constant value of the beta factor to determine the intrinsic mechanical quantities is an acceptable hypothesis.

From these last results dealing with the specific influence of the evolution of the beta factor with stretching in the case of HDPE, we now consider a constant value of the beta factor during the stretching procedure for our three polymer matrices.

4.3. Determination of the true intrinsic mechanical behaviours

The microscopic observations of damage after stretching of PP/EPR, PET (Figures 5 and 6) and HDPE (Figure 7) enable the choice of the most suitable β factor in the determination of the intrinsic true behaviour. In the case of PP/EPR, a β factor tending toward infinity is used due to the presence of cigar-like voids. For HDPE, a β factor of 1 is retained because of the development of bubble-like voids. For PET, the chosen β factor is 0 due to the presence of crazes having a penny shape. Using the equations described previously, the intrinsic true mechanical behaviours of each polymer are presented in figure 11.

These corrections eliminate the anomalies observed in the case of the overall true behaviours directly obtained by means of the VideoTraction™ system. The curves calculated either at three different true strain rates (PP/EPR and PET) or three different temperatures (HDPE) are finally really stackable. The use of the phenomenological law of G'sell and Jonas (1979) is now suitable for simulation and prediction of the mechanical properties of these thermoplastics because no more curves intersection exists (Ponçot *et al.*, 2009; Ponçot, 2009).

4.4. Comparison of the equivalent true intrinsic mechanical behaviours between various deformation paths using the Von Mises plastic criterion:

In order to compare the mechanical behaviours of the materials in uniaxial tension, plane tension and simple shear, we applied the plastic criterion of Von Mises taking the

conventional uniaxial tensile test as reference. The deduced expressions of the true intrinsic stress and strain are:

- For plane tensile test: $\varepsilon^{i}_{33\,equ} = \frac{2}{\sqrt{3}}\varepsilon^{i}_{33}$ and $\sigma^{i}_{33\,equ} = \frac{\sqrt{3}}{2}\sigma^{i}_{33}$,
- For simple shear test: $\varepsilon_{equ} = \frac{\gamma}{\sqrt{3}}$ and $\sigma_{equ} = \tau.\sqrt{3}$.

Figure 12 presents the differences between the true mechanical behaviours (a) and the equivalent true intrinsic mechanical behaviours (b) in the case of PP/EPR material deformed based on these three deformation paths. The integration of the volume strain taking into account the cavities shape gives results which are in good agreement with the previous simulations (Hervé *et al.*, 1993 and 1995) and experiments brought by G'sell *et al.* (1994, 1997, 1999) in the case of HDPE. The behaviours in uniaxial tension and simple shear are the two extreme ones in terms of stress since all the other simple or complex mechanical paths behaviours are encountered between pure tension and pure shear (Dahoun, 1992; G'sell *et al.*, 1997 and 1999). This means that damage is maximum in tension and minimum in shear. The behaviour in plane tension is below the one of tension since the hydrostatic pressure remains weak for the kind of sample geometry used to perform the tests. We notice that the curves are similar until the beginning of the strain-hardening. It informs us that the micromechanisms of deformation involved at this early stage of deformation are comparable whatever the mechanical path. It confirms the fact that the real influence of the volume damage on the mechanical behaviour happens during the plastic deformation of the material. Before, deformation of polymer is essentially governed by interlamellar and interchains shearing inducing creation of shear bands (Baltá-Calleja *et al.*, 1970; Kaufman *et al.*, 1973) localized in the amorphous phase. Similar results in the case of PET and HDPE were provided (G'sell *et al.*, 1999; Addiego, 2006; Ponçot *et al.*, 2011).

5. Conclusion:

In this paper, we develop a methodology which enables the determination of the true intrinsic mechanical behaviour of thermoplastic polymers from the overall behaviour, volume strain and voids shape factor. To this end, we selected two semi-crystalline polymers (polypropylene/ethylene-propylene rubber, PP/EPR and high-density polyethylene, HDPE) and one amorphous polymer (polyethylene terephtalate, PET). The VidéoTraction™ system was used in tension to determine the overall behaviour of the materials, i.e. the true stress – true strain curves and the volume strain – true strain curves. Attention was also focused on the impact of strain rate and temperature on the tensile behaviour of the materials. The void shape of the materials was examined at the *post mortem* state by scanning electron microscopy and optical microscopy. At high strain rate, volume damage is the most important microstructural modification since polymer chains do not have enough time to accommodate to the macroscopic strain by an orientation process. The higher the temperature (compared to the glass temperature of the material), the more important is the orientation of the macromolecular chains along the stretching direction. Actually, this is due to an increase of chain mobility since the material is in its viscoelastic state. In these last conditions, volume damage is relatively weak. Consequently, there is a strong competition between orientation of the macromolecular chains and damage characterized by the creation of voids inside the polymer. It results that raw tensile curves $\sigma_{33} = f(\varepsilon_{33})$ recorded by means of the optical system are not stackable for large true strain values when strain-hardening occurs. It means that the modification of one test parameter does not affect the true mechanical behaviour in the same manner from the elastic to the plastic regions. Intersections between true stress-strain curves are observed and make impossible the simulation of these curves using phenomenological constitutive equations. Microstructure observations reveal that cavities do not develop in the same manner for all the investigated materials. PP/EPR presents cigars or tubes oriented in the stretching direction, HDPE shows bubbles characteristic of an isotropic volume damage and PET is damaged by crazes perpendicular to the tension direction. Thus, based on our observations, a form factor called β was introduced in the determination of the true intrinsic mechanical behaviours of polymers $\sigma_{33}^{i} = f(\varepsilon_{33}^{i})$. The calculated intrinsic tensile curves exhibit no irregularity (stackable curves), and hence, can be easily fitted by a phenomenological model such as the G'sell and Jonas law (G'sell and Jonas, 1979; Ponçot, 2009). The determination of the true intrinsic mechanical behaviours enables the comparison of different deformation paths based on the plastic criterion of Von Mises used to determine the equivalent behaviours. Thus, we calculated the equivalent true intrinsic simple shear and plane tension behaviours based on the true intrinsic tensile behaviour. These three behaviours are similar prior up to yield point. Similarities of the micromechanisms of deformation involved during solicitation of amorphous and semi-crystalline polymers before plasticity of the material are enlightened.

Acknowledgements:

The previous works of Professor G'sell Christian on polymers plasticity and his precious and judicious ideas are greatly honoured in this paper.

References:

Addiego, F., Dahoun, A., G'sell, C., Hiver, J.M., 2006. Characterization of volume strain at large deformation under uniaxial tension in high-density polyethylene. Polymer 47 (12), 4387 – 4399.

Addiego, F., Dahoun, A., G'sell, C., Hiver, J.M., 2006. Volume Variation Process of High-Density Polyethylene During Tensile and Creep Tests. Oil & Gas Science and Technology 61 (6), 715 – 724.

Addiego, F., 2006. Caractérisation de la variation volumique du polyéthylène au cours de la déformation plastique en traction et en fluage. Ph. D. Thesis, INPL (Nancy).

Addiego, F., Di Martino, J., Ruch, D., Dahoun, A., Godard, O., Patlazhan, S., 2011. Quantification of cavitation in neat and calcium carbonate-filled high-density polyethylene subjected to tension. Journal of Engineering Materials and Technology 133, 030904.1 – 7.

Amornsakchai, T., Olley, R.H., Basset, D.C., Al-Hussein, M.O.M., Unwin, A.P., Ward, I.M., 2000. On the influence of initial morphology on the internal structure of highly drawn polyethylene. Polymer 41 (23), 8291 – 8298.

Ayoub, G., Zaïri, F., Naït-Abdelaziz, M., Gloaguen, J.M., 2010. Modelling large deformation behaviour under loading-unloading of semi-crystalline polymers: Application to high density polyethylene. International Journal of Plasticity 26, 329 – 347.

Ayoub, G., Zaïri, F., Fréderix, C., Gloaguen, J.M., Naït-Abdelaziz, M., Seguela, R., Lefebvre, J.M., 2011. Effects of crystal content on the mechanical behaviour of polyethylene under finite strins: Experiments and constitutive modelling. International Journal of Plasticity 27, 492 – 511.

Ahzi, S., Makradi, A., Gregory, R.V., Edie, D.D., 2003. Modeling of deformation behavior and strain-induced crystallization in poly(ethylene terephthalate) above the glass transition temperature. Mechanics of Materials 35, 1139 – 1148.

Baltá-Calleja F.J., Peterlin, A., 1970. Plastic deformation of polypropylene: VI : Mechanisms and properties. Journal of Macromolecular Science - Physics B4-3, 519 – 540.

Bartczak, Z., Galeski, A., Argon, A.S. et Cohen, R.E., 1996. On the plastic deformation of the amorphous component in semicrystalline polymers. Polymer 37, 2113 – 2123.

Beremin, F.M., 1980. Elastoplastic calculations using the finite element method of circumferentially notched axisymmetric specimens. Journal de Mécanique appliquée 4(3), 307 – 325.

Boisot, G., Laiarinandrasana, L., Besson, J., Fond, C., Hochstetter, G., 2011. Experimental investigations and modeling of volume change induced by void growth in polyamide 11. International Journal of Solids and Structures 48, 2642 – 2654.

Boyce, M.C., Arruda, E.M., 1990. An experimental and analytical investigation of the large strain compressive and tensile response of glassy polymers. Polymer Engineering and Science 30, 1288 – 1298.

Boyce, M.C., Socrate, S., Llana, P.G., 2000. Constitutive model for the finite deformation stress–strain behavior of poly(ethylene terephthalate) above the glass transition. Polymer 41, 2183 – 2201.

Bridgman, PW, 1952. The effect of nonuniformities of stress at the neck of a tension specimen, in large plastic flow and fracture. Metallurgy and metallurgical engineering series, First edition, New York, McGraw-Hill book company, Inc., 9 – 37.

Bucknall, C.B., Clayton, D., Wendy, E. Keast, 1972. Rubber-toughening of plastics, part 1: Creep mechanisms in HIPS. Journal of Materials Science 7 (12), 202 – 210.

Chaboche, J.L., 1995. Formalisme général des lois de comportement : applications aux métaux et polymères. Introduction à la mécanique des polymères, C. G'sell and J.M. Haudin (INPL), 119-140.

Dahoun, A., 1992. Comportement plastique et textures de déformation des polymères semi-cristallins en traction uniaxiale et en cisaillement simple. Thèse de doctorat de l'Ecole des Mines de Nancy - INPL, Spécialité «Sciences et Génie des Matériaux».

Dahoun, A., 2004. Etude des mécanismes de déformation et d'endommagement plastique des polymères solides. Habilitation à Diriger des Recherches, INPL (Nancy).

Detrez, F., Cantournet, S., Seguela, R., 2011. Plasticity/damage coupling in semi-crystalline polymers prior to yielding: Micromechanisms and damage law identification. Polymer 52, 1998 – 2008.

Galeski, A. and Rozanski, A., 2010. Cavitation during Drawing of Crystalline Polymers. Macromolecular Symposia 298, 1 – 9.

G'sell C., Jonas, J.J., 1979. Determination of the plastic behavior of solid polymers at constant true strain rate. Journal of Materials Science 14 (3), 583 – 591.

G'sell, C., Hiver, J.M., Dahoun, A., Souahi, A., 1992. Video-controlled tensile testing of polymers and metals beyond the necking point. Journal of Materials Science 27, 5031 – 5039.

G'sell, C., Dahoun, A., 1994. Evolution of microstructure in semi-crystalline polymers under large plastic deformation. Materials Science and Engineering A175, 183 – 199.

G'Sell, C., Dahoun, A., Favier, V., Hiver, J.M., Philippe, M.J., Canova, G.R., 1997. Microstructure transformation and stress-strain behavior of isotactic polypropylene under large plastic deformation. Polymer Engineering and Science 37 (10), 1702 – 1711.

G'sell, C., Dahoun, A., Royer, F.X., Philippe, M.J., 1999. The influence of the amorphous matrix on the plastic hardening at large strain of semicrystalline polymers. Modeling Simulation Materials Science Engineering 7, 817 – 828.

G'sell, C., Hiver, J.M., Dahoun, A., 2002. Experimental characterization of deformation damage in solid polymers under tension and its interrelation with necking. International Journal of Solids and Structures, 39 (13-14). 3857 – 3872.

Gologanu, M., Leblond, J.B., Perrin, G., Devaux, J., 1997. Recent extensions of Gurson's model for porous ductile metals. In: Suquet, P. (Ed.), Continuum Micromechanics. Springer-Verlag, Berlin, 61 – 130.

Gurson, A.L., 1977. Continuum theory of ductile rupture by void nucleation and growth: Part I – Yield criteria and flow rules for porous ductile media. Journal of Engineering Materials and Technology 99, 2 – 15.

Hervé, E., Zaoui, A., 1993. n-Layered inclusion-based micromechanical modelling. International Journal of Engineering Science 31 (1), 1 – 10.

Hervé, E., Zaoui, A., 1995. Elastic behavior of multiply coated fibre-reinforced composites. I International Journal of Engineering Science 33 (10), 1419–1433.

Kaufman, W.E., Schultz, J.M., 1973. Lamellar and interlamellar structure in melt-crystallized polyethylene. Journal of materials science 8 (1), 41 – 46.

Khan, A., Zhang, H., 2001. Finite deformation of a polymer: experiments and modelling. International Journal of Plasticity 17, 1167 – 1188.

Khan, A.S., Lopez-Pamies, O., Kazmi, R., 2006. Thermo-mechanical large deformation response and constitutive modeling of viscoelastic polymers over a wide range of strain rates and temperatures. International Journal of Plasticity 22, 581 – 601.

Laiarinandrasana, L., Besson, J., Lafarge, M., Hochstetter, G., 2009. Temperature dependent mechanical behaviour of PVDF: experiments and numerical modelling. International Journal of Plasticity 25, 1301 – 1324.

Lemaitre, J., 1996. A course on damage mechanics. Springer (Berlin).

Mae, H., Omiya, M., Kishimoto, K., 2008. Microstructural observation and simulation of micro damage evolution of ternary polypropylene blend with ethylene-propylene-rubber (EPR) and talc. Journal of Solid Mechanics and Materials Engineering 2 (8), 1018 – 1036.

Martin, J., Ponçot, M., Bourson, P., Dahoun, A., Hiver, J.M., 2011. Study of the Crystalline Phase Orientation in Uniaxially Stretched Polypropylene by Raman Spectroscopy: Validation and Use of a Time-Resolved Measurement Method. Polymer Engineering and Science 51 (8), 1607-1616.

Naqui, S.I., Robinson, I.M., 1993. Review tensile dilatometric studies of deformation in polymeric materials and their composites. Journal of Materials Science, 28, 1421 – 1429.

Nikolov, S., Lebensohn, R.A., Raabe, D., 2006. Self-consistent modeling of large plastic deformation, texture and morphology evolution in semi-crystalline polymers. Journal of the Mechanics and Physics of Solids 54, 1350 – 1375.

Nitta, K.H., Yamaguchi, M., 2008. Morphology and mechanical properties in blends of polypropylene and polyolefin-based copolymers. Polyolefin Blends, D. Nwabunma and T. Kyu, Willey (New York), 224 – 268.

Olley, R.H., Basset, D.C., 1982. An improved permenganic etchant for polyolefines. Polymer 23 (12), 1707 – 1710.

Plummer, C.J., Jr., Kausch, H.H., 1996. Deformation and entanglement in semi-crystalline polymers. Journal of Macromolecular Science - Physics B35 (3, 4), 637 – 657.

Ponçot, M., Dahoun, A., Hiver, J.M., Verchère, D., Doux, M., Lucchini, L., 2009. Thermomecanical behaviour of metal/polymer composites along different deformation paths: Determination of intrinsic mechanical behaviour laws on polymer film. DYFP2009 (14th edition) - Book of Abstracts, 435 – 438.

Ponçot, M., 2009. Comportements thermomécaniques de polymères chargés selon différents chemins de déformation et traitements thermiques. Ph. D. Thesis, INPL (Nancy).

Ponçot, M., Martin, J., Godard, O., Hiver, J.M., Dahoun, A., Bourson, P., 2011. Mécanismes de déformation plastique en traction et cisaillement de PET amorphe extrudé. Matériaux & Techniques "in press".

Ponçot, M., Martin, J., Hiver, J.M., Verchère, D., Dahoun, A., 2011. Study of the dimensional instabilities of laminated polypropylene films during heating treatments. Journal of applied polymer science, DOI: 10.1002/app.36450.

Pukanszky, B., Van Es, M., Mauer, F.H.J., Voros, G., 1994. Micromechanical deformations in particulate filled thermoplastics: volume strain measurements. Journal of Materials Science, 29 (9), 2350 – 2358.

Richeton, J., Ahzi, S., Vecchio, K.S, Jiang, F.C., Makradi, A., 2007. Modeling and validation of the large deformation inelastic response of amorphous polymers over a wide range of temperatures and strain rates. International Journal of Solids and Structures 44, 7938 – 7954.

Samuels, R.J., 1971. Plastic Deformation of Polymers. M. Dekker (New York).

Samuels, R.J., 1974. Structured Polymer Properties: The Identification, Interpretation, and Application of Crystalline Polymer Structure. Wiley (New York).

Séguela R., 2007. On the natural draw ratio of semi-crystalline polymers: review of the mechanical, physical and molecular aspects. Macromolecular Material Engineering 292, 235 – 244.

Steenbrink, A.C., Van der Giessen, E., Wu, P.D., 1997. Void growth in glassy polymers. Journal of the Mechanics and Physics of Solids 45 (3), 405 – 437.

Tvergaard, V., 1981. Influence of voids on shear band instabilities under plane strain conditions. International Journal of Fracture 17, 389 – 407.

Uchida, M., Tada, N., 2011. Sequential evaluation of continuous deformation field of semi-crystalline polymers during tensile deformation accompanied by neck propagation. International Journal of Plasticity 27, 2085 – 2102.

van der Wal, A., Gaymans R.J., 1999. Polypropylene-rubber blends: 5. Deformation mechanism during fracture. Polymer 40, 6067 – 6075.

Vigny, M., Aubert, A., Hiver, J. M., Aboulfaraj, M., G'sell, C., 1999. Constitutive viscoplastic behavior of amorphous PET during plane-strain tension stretching, Polymer Engineering and Science 39 (12), 2366 – 2376.

Ward, I.M., 1971. Mechanical Properties of Solid Polymers. Wiley (London).

Wunderlich, B., 1973. Macromolecular physics: Crystal structure, morphology, defects. Academic Press (New York).

Zaïri, F., Naït-Abdelaziz, M., Woznica, K., Gloaguen, J.M., 2005. Constitutive equations for the viscoplastic-damage behaviour of a rubber-modified polymer. European Journal of Mechanics A/Solids 24, 169 – 182.

Zaïri, F., Naït-Abdelaziz, M., Woznica, K., Gloaguen, J.M., 2007. Elasto-viscoplastic constitutive equations for the description of glassy polymers behavior at constant strain rate. Journal of Engineering Materials and Technology 129, 29 – 35.

Zaïri, F., Naït-Abdelaziz, M., Gloaguen, J.M., Lefebvre, J.M., 2008. Modelling of the elasto-viscoplastic damage behaviour of glassy polymers. International Journal of Plasticity 24, 945 – 965.

Zaïri, F., Naït-Abdelaziz, M., Gloaguen, J.M., Lefebvre, J.M., 2011. A physically-based constitutive model for anisotropic damage in rubber-toughened glassy polymers during finite deformation. International Journal of Plasticity 27, 25 – 51.

Figure captions:

Figure 1: True tensile behaviors as a function of the true strain rate in the case of a) PP/EPR and b) PET (tensile anomalies are indicated by an ellipsoid).

Figure 2: True tensile behaviors as a function of temperature in the case of HDPE (tensile anomalies are indicated by an ellipsoid).

Figure 3: Evolution of the volume strain as a function of the true strain rate in case of a) PP/EPR and b) PET.

Figure 4: Evolution of the volume strain in function of the temperature in case of stretched HDPE.

Figure 5: SEM micrographies of the RVE of PP/EPR tensile specimens uniaxially stretched at 30 °C and $\dot{\varepsilon} = 5.10^{-3}\ s^{-1}$ (the stretching direction is vertical).

Figure 6: Optical micrographies taken on 20 µm-thick slices of the RVE of PET specimens uniaxially stretched at 50°C and $5.10^{-5}\ s^{-1}$ (the stretching direction is vertical).

Figure 7: SEM micrographies of the RVE of HDPE probes uniaxially stretched at 25 °C and $10^{-3}\ s^{-1}$ (the stretching direction is vertical) (Addiego *et al.*, 2006).

Figure 8: Damaged polymers are considered as a two-phase system.

Figure 9: Remarkable values of the β factor linked with current cavities shapes observed in uniaxially stretched polymers.

Figure 10: a) Impact of the three different remarkable values of the β factor on the final intrinsic true mechanical behavior of HDPE and, b) experimental evolution of the beta factor as a function of the volume strain.

Figure 11: True intrinsic mechanical behaviors in uniaxial tension of a) PP/EPR, b) PET and c) HDPE taking into account volume strain and voids shape (β form factor).

Figure 12: a) Equivalent true mechanical behaviors and b) Equivalent true intrinsic mechanical behaviors of PP/EPR using the plastic criterion of Von Mises. Comparison of three deformation paths: uniaxial tension, plane tension and simple shear.

Figure

Click here to download high resolution image

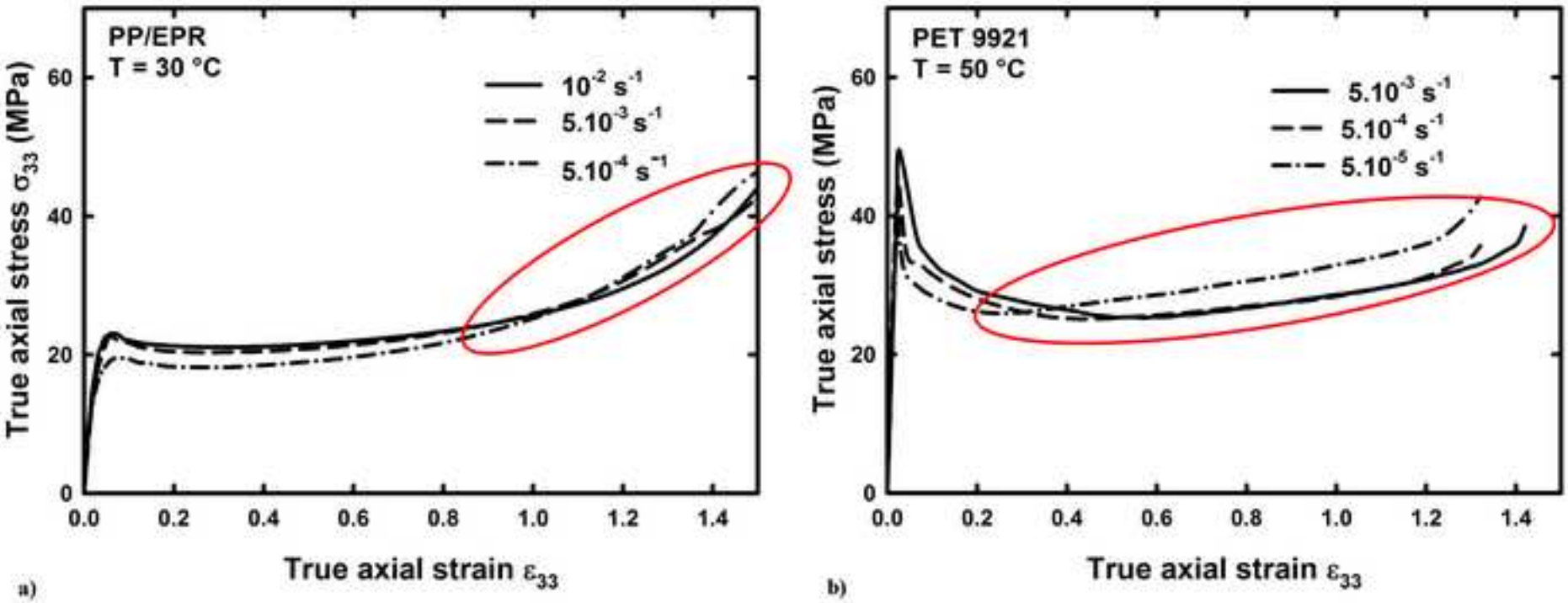

Figure

Click here to download high resolution image

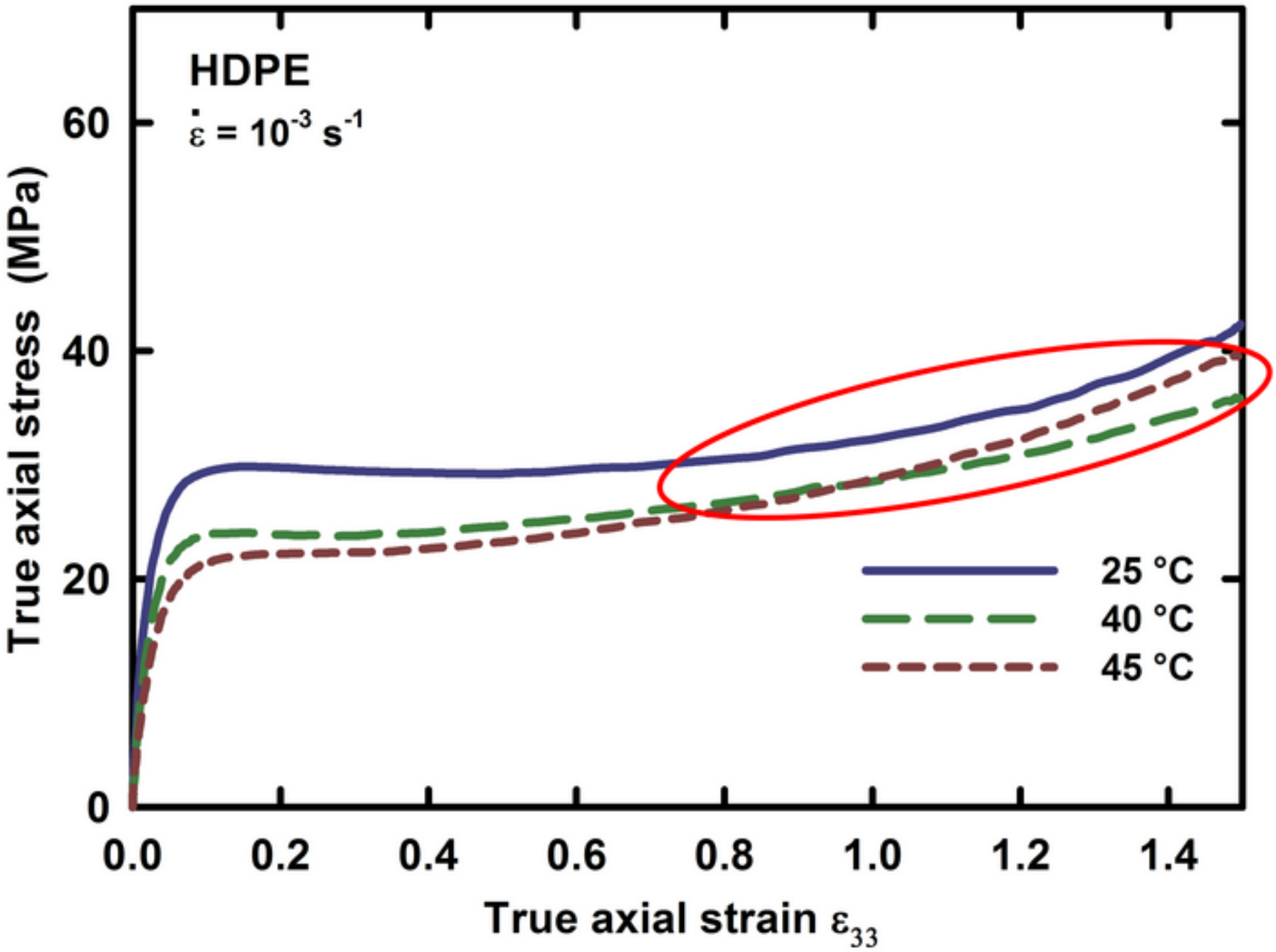

Figure
Click here to download high resolution image

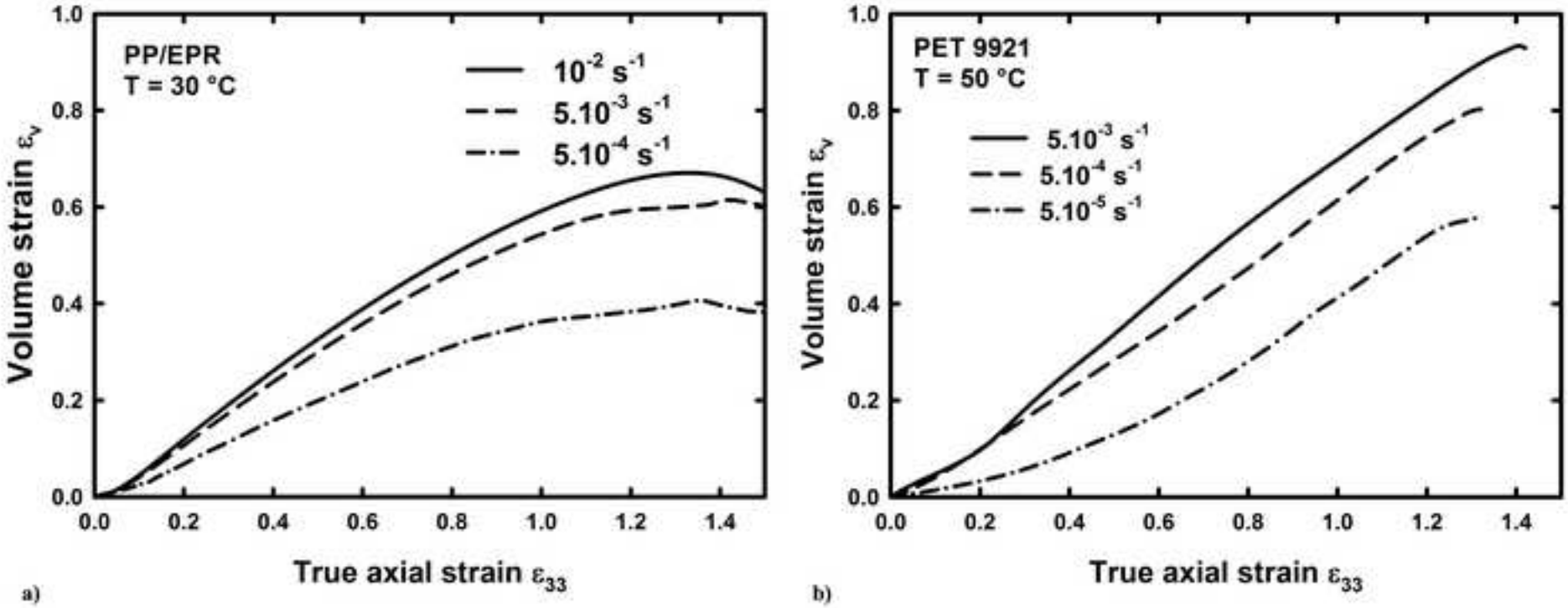

Figure
Click here to download high resolution image

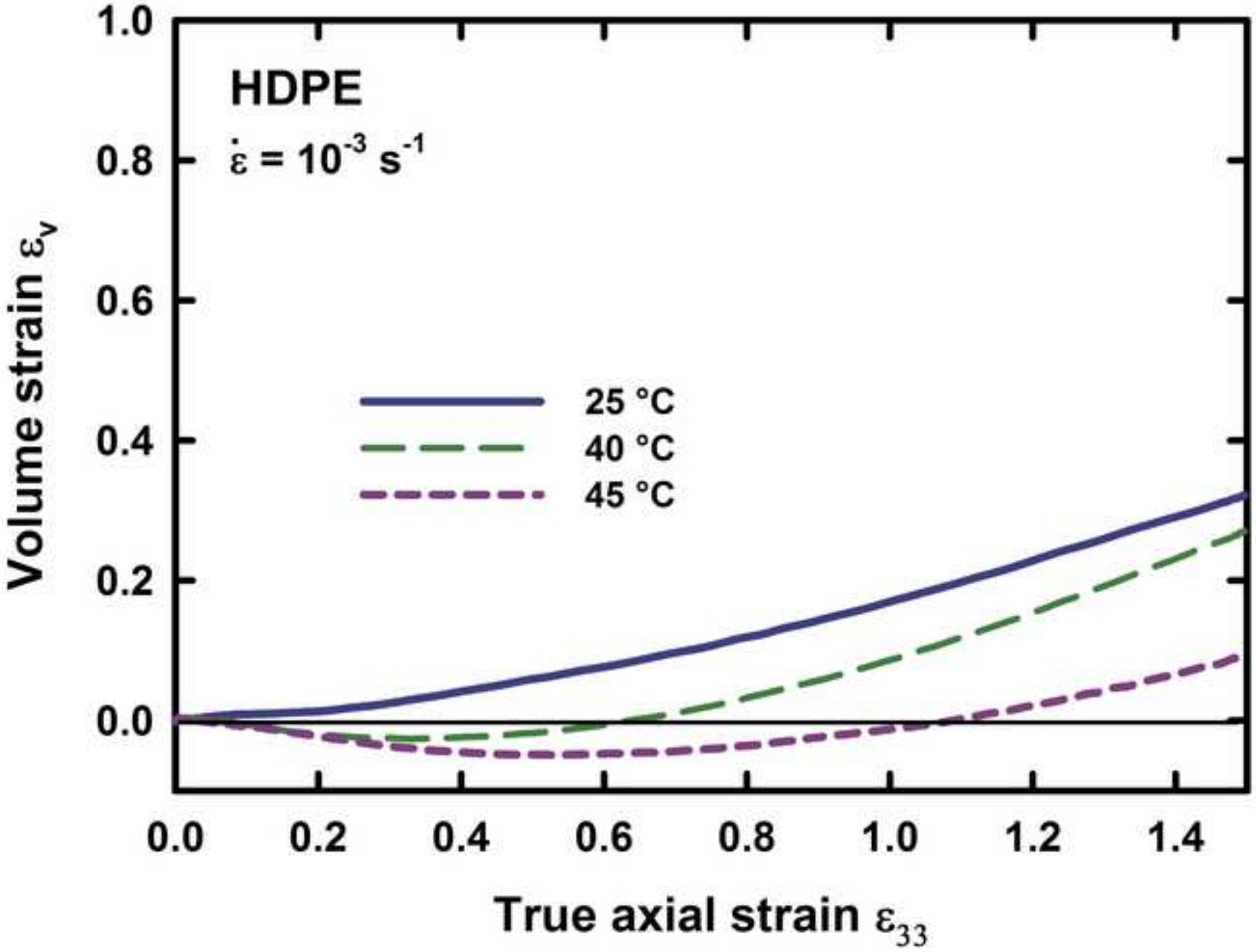

Figure

Click here to download high resolution image

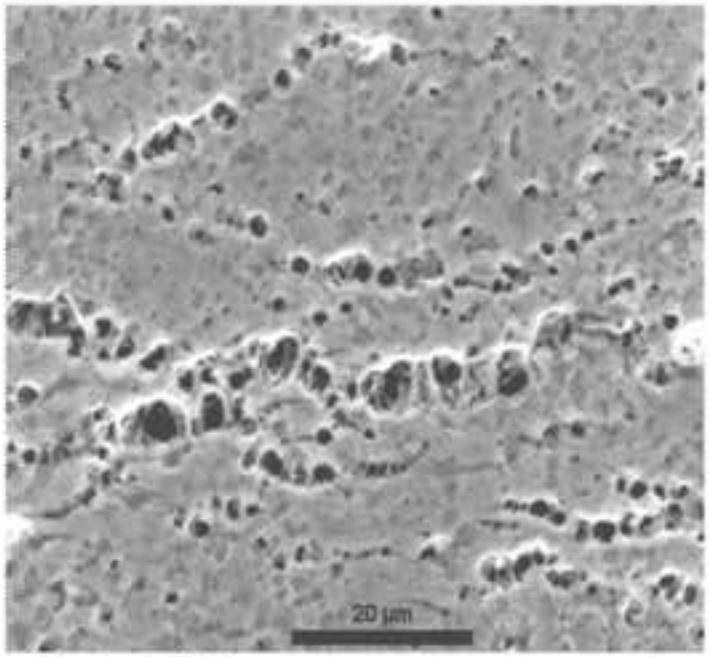

a) $\varepsilon_{33} = 0.3$

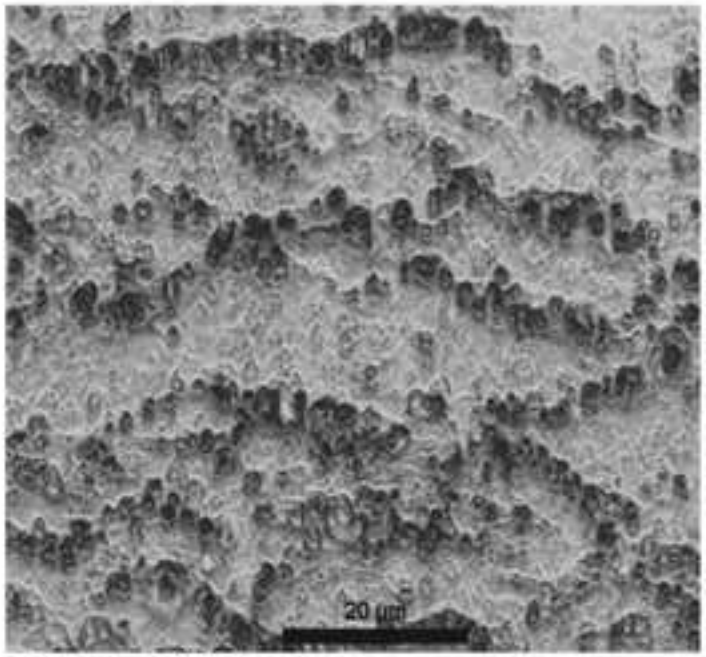

b) $\varepsilon_{33} = 0.5$

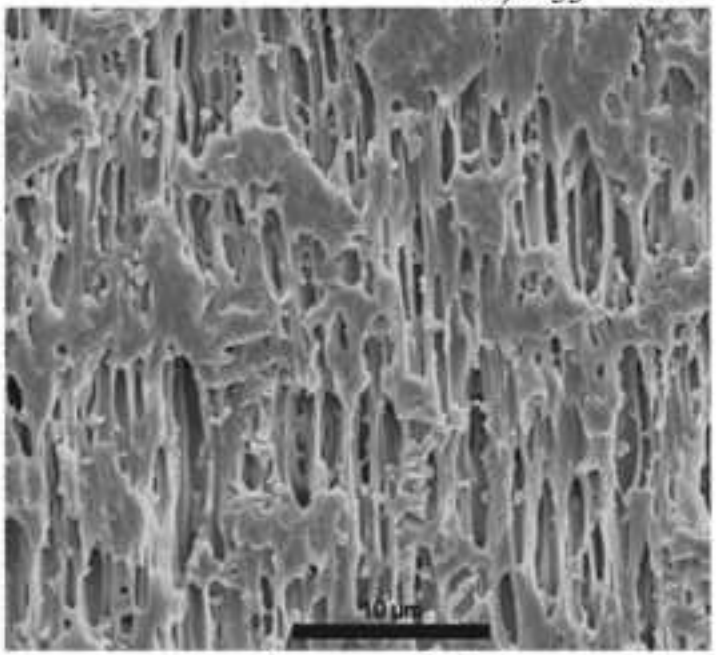

c) $\varepsilon_{33} = 1.4$

Figure
Click here to download high resolution image

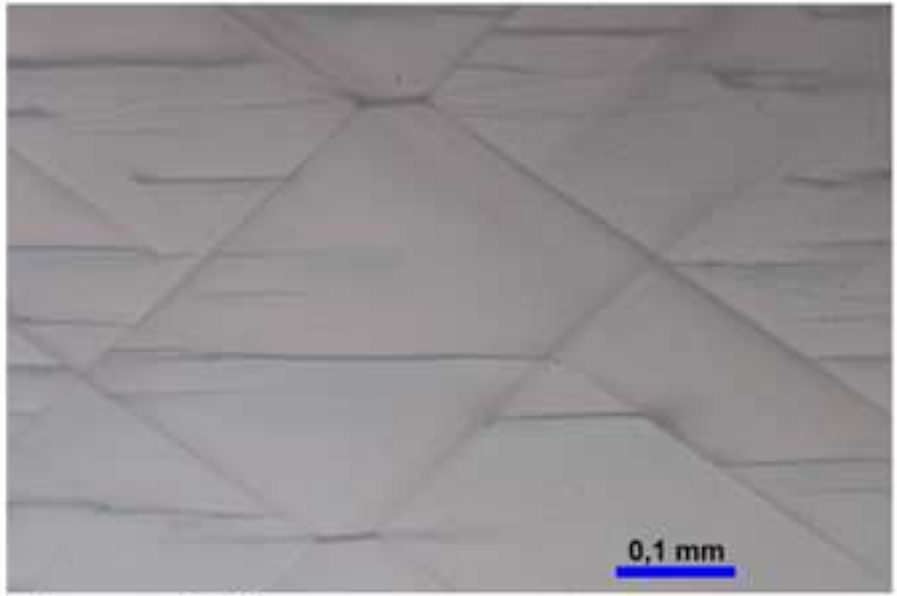

a) $\varepsilon_{33} = 0.45$

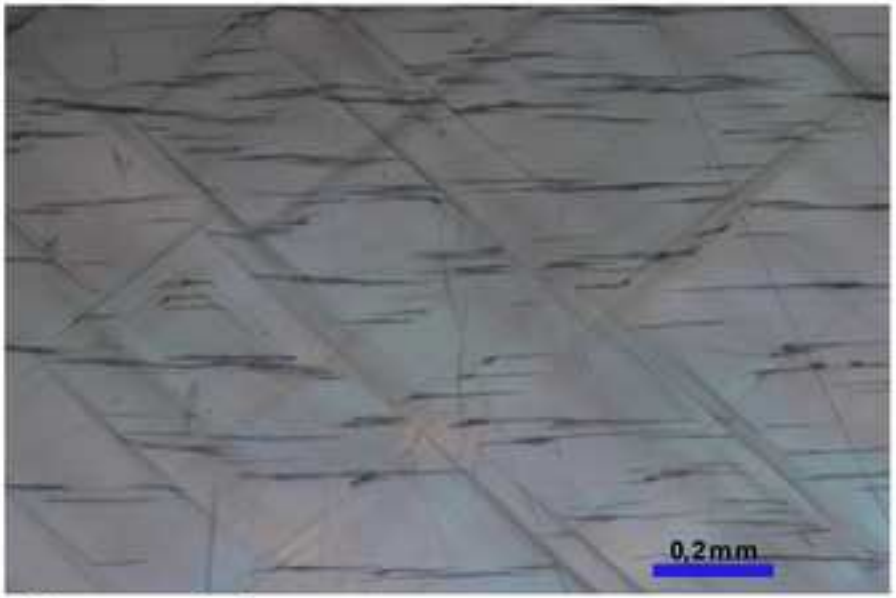

b) $\varepsilon_{33} = 1.2$

Figure
Click here to download high resolution image

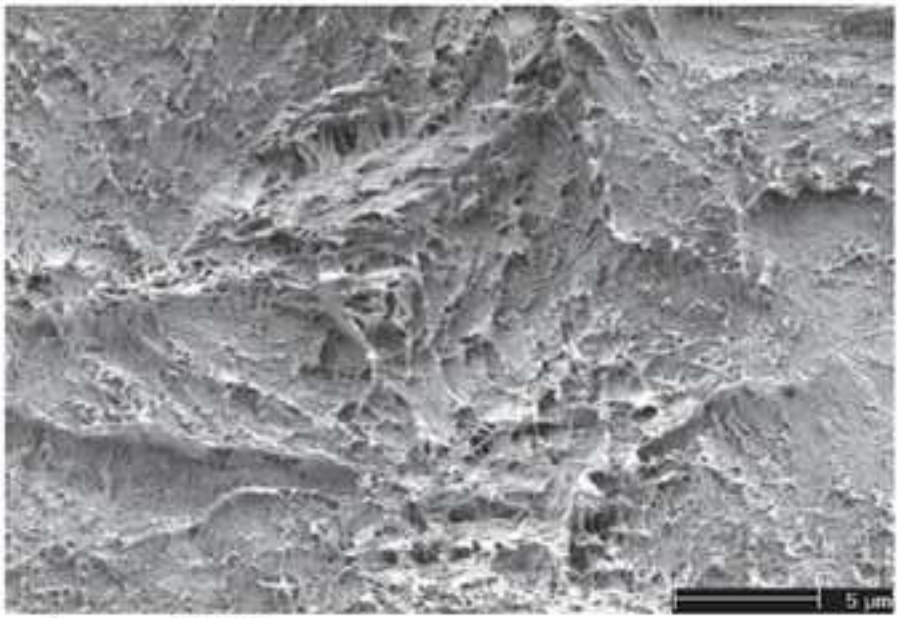

a) $\varepsilon_{33} = 0.29$

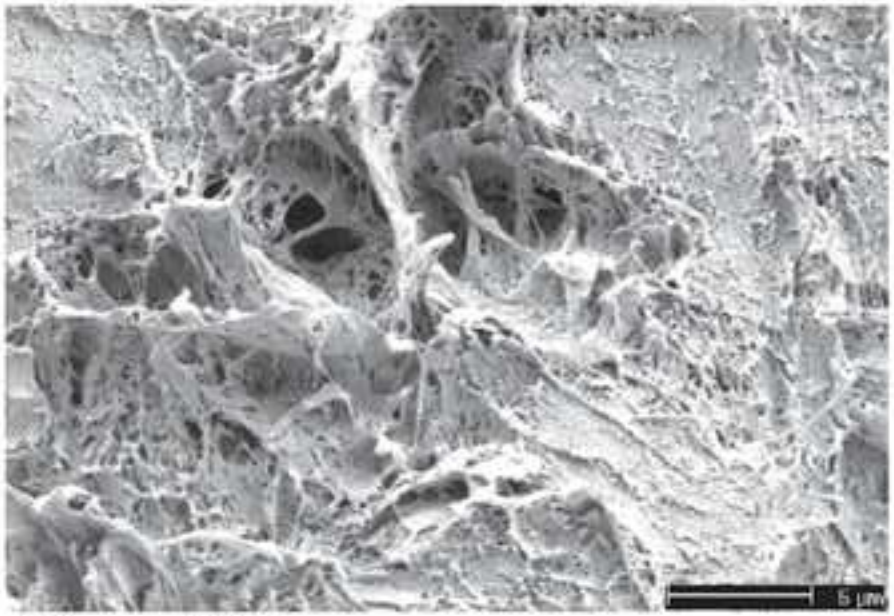

b) $\varepsilon_{33} = 0.48$

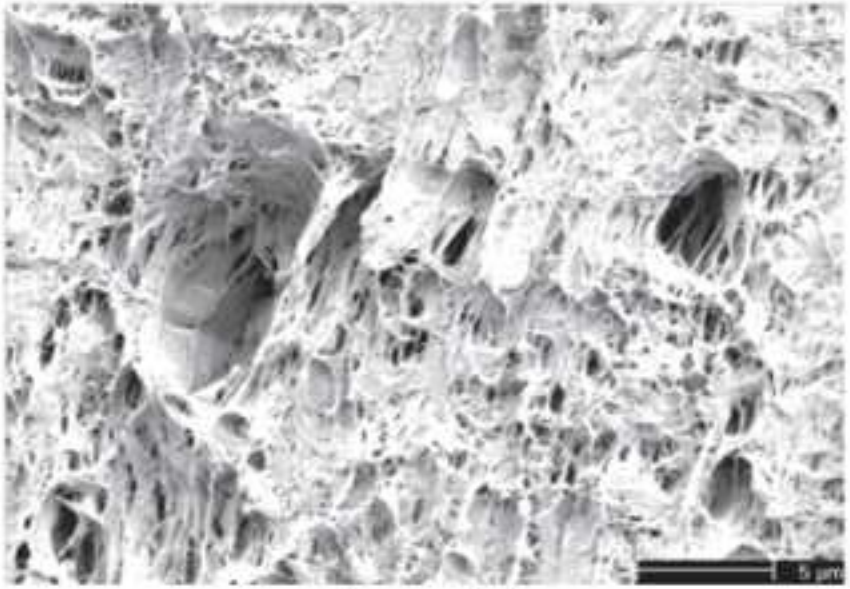

c) $\varepsilon_{33} = 1.3$

Figure
Click here to download high resolution image

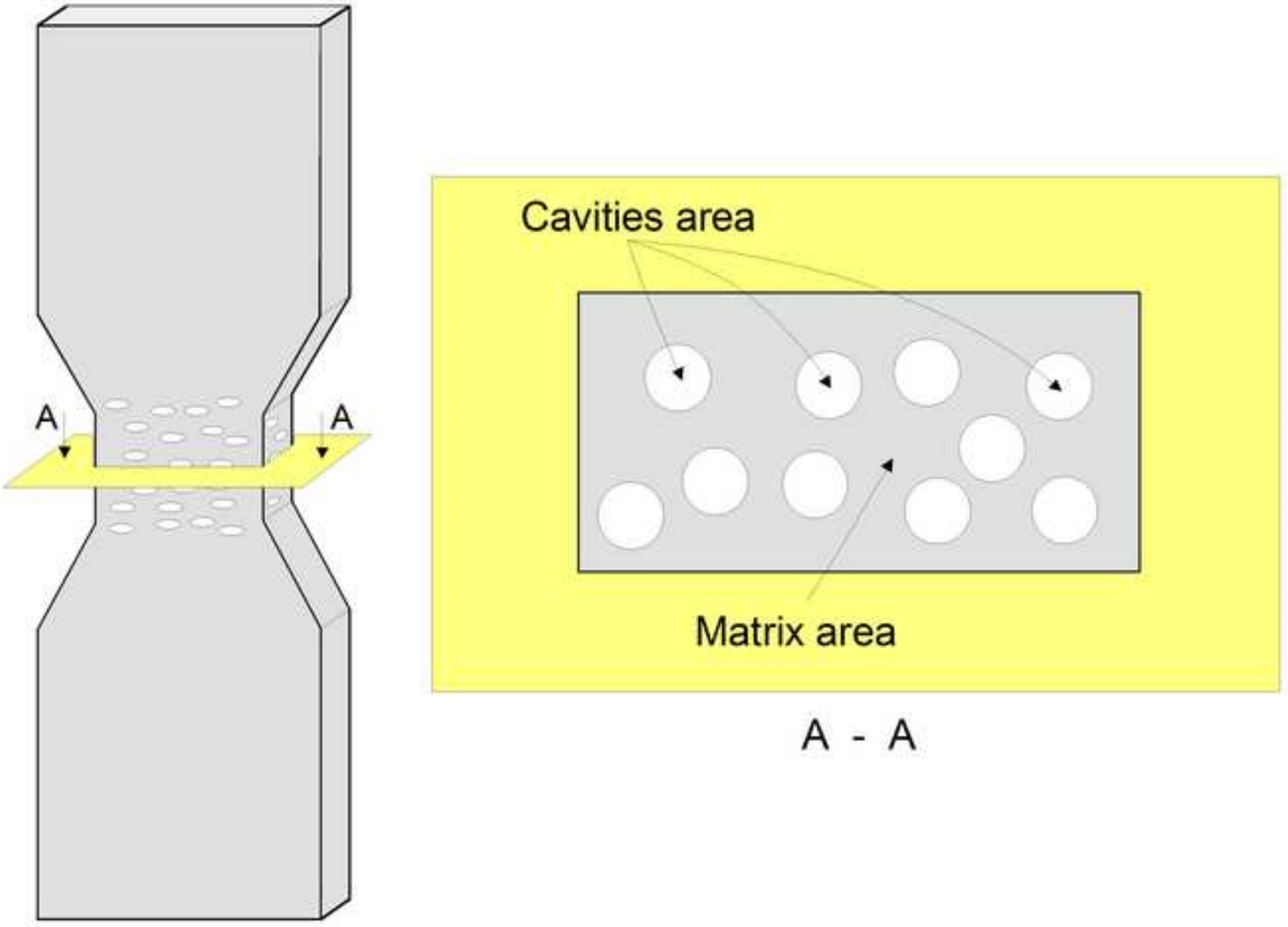

Figure

Click here to download high resolution image

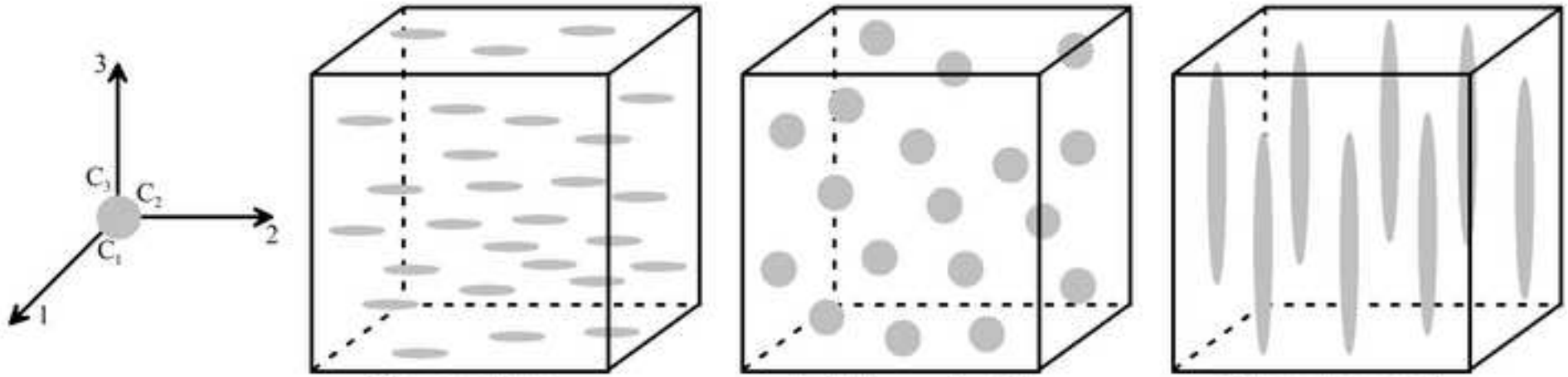

Figure
Click here to download high resolution image

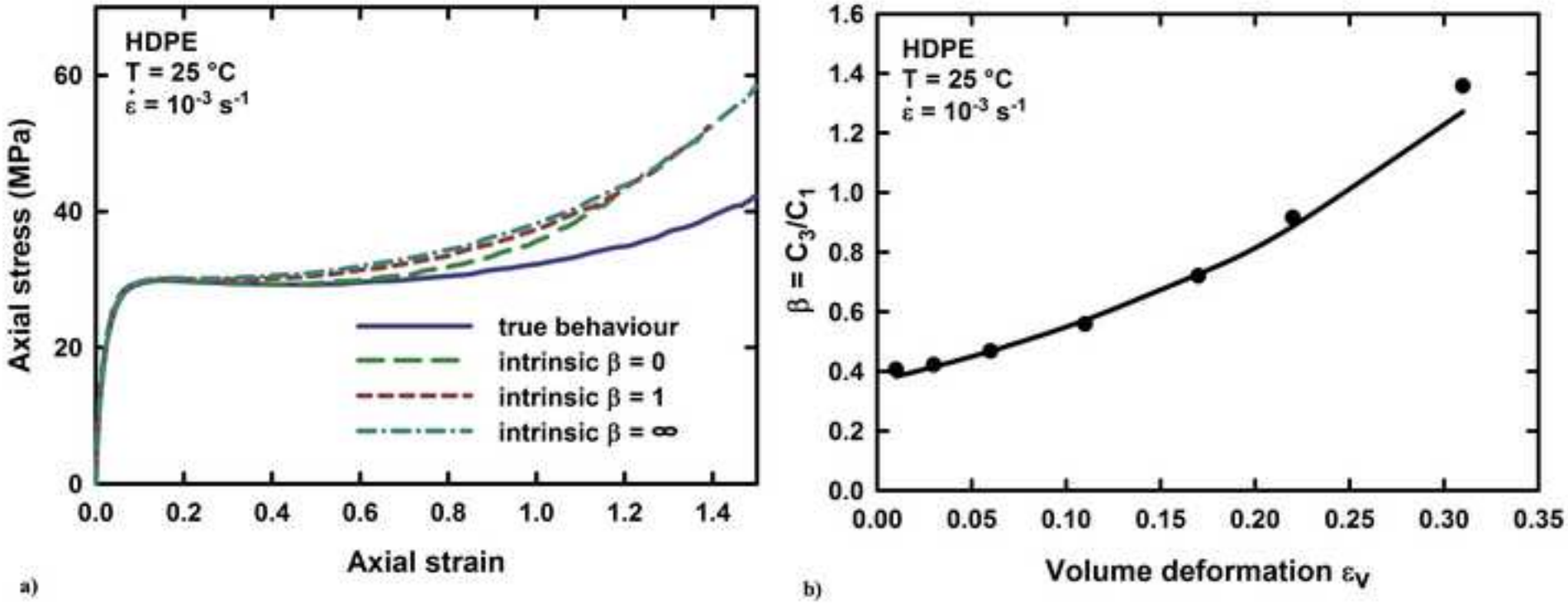

Figure

Click here to download high resolution image

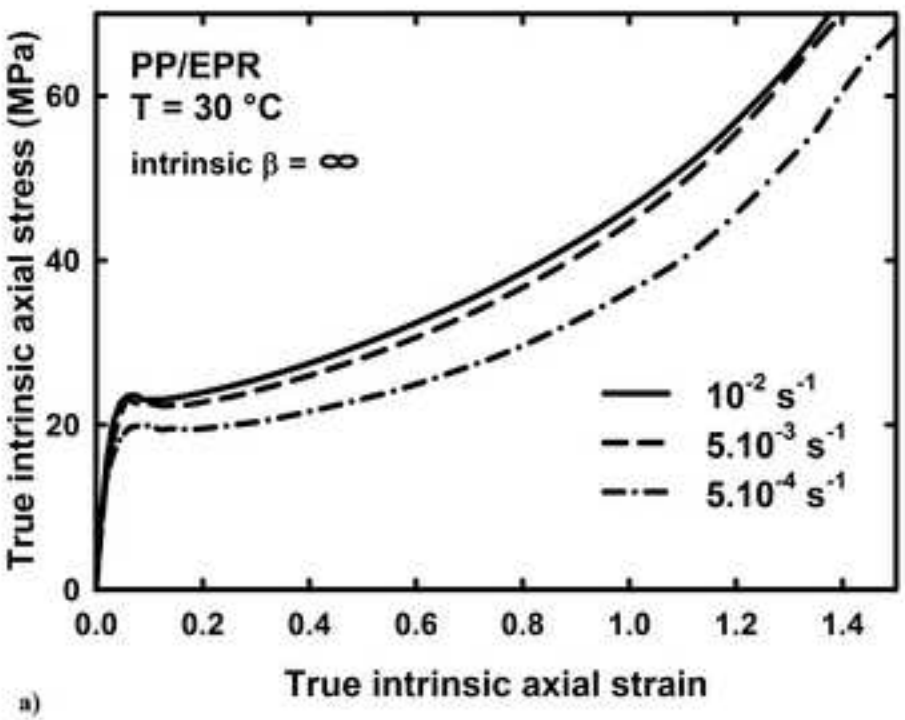

a)

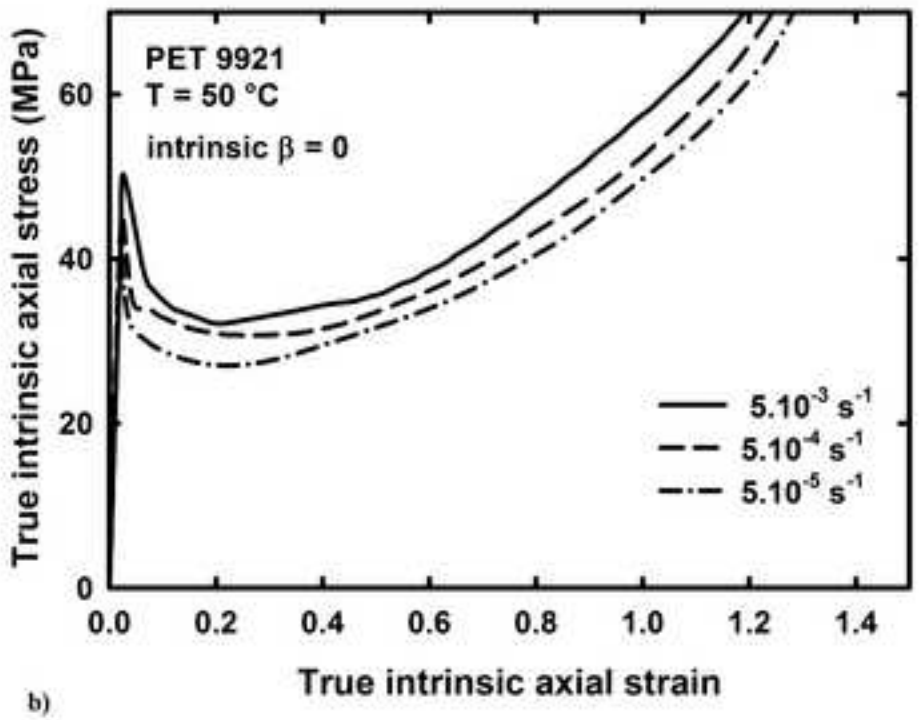

b)

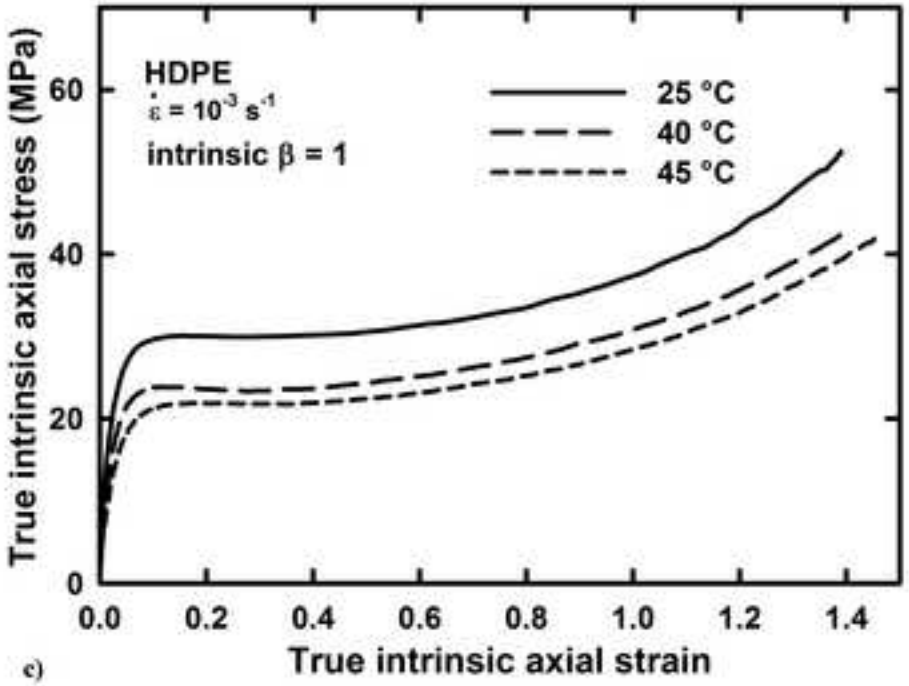

c)

Figure
Click here to download high resolution image